Research paper

Struct Multidisc Optim 26, 209–218 (2004)
DOI 10.1007/s00158-003-0340-5

Topology synthesis of electrothermal compliant mechanisms using line elements*

N.D. Mankame, G.K. Ananthasuresh

Abstract This paper presents a *line-element*-based approach to the topology synthesis of electrothermal compliant (ETC) mechanisms. A line element is a one-dimensional model of the electrical, thermal, and elastic behavior of a beam-like continuum. In contrast to topology synthesis of ETC mechanisms by a continuum-element-based approach, the line-element-based approach offers significant conceptual and practical advantages. The line element allows for straightforward modeling of surface heat transfer in the topology optimization framework. It also obviates the need to interpolate electrical and thermophysical properties in the topology synthesis procedure. Moreover, this approach results in clean geometries that are easy to fabricate directly in their optimized form.

Solutions obtained from this procedure are compared with results from continuum-based optimal synthesis procedures as well as intuitive designs reported in the literature. A number of design examples are used to demonstrate the ability of the procedure to generate nonintuitive topologies. The synthesis procedure is also used to study the influence of the direction of output and the electrical and thermal resistance of the workpiece on the resulting optimal topologies.

Key words ETC, compliant mechanisms, topology optimization, electro-thermal actuation

Received: 19 October 2001
Published online: 23 December 2003

N.D. Mankame✉, G.K. Ananthasuresh

Department of Mechanical Enginnering and Applied Mechanics, University of Pennsylvania, Philadelphia, PA 19104, USA
e-mail: (nileshdm, gksuresh)@seas.upenn.edu

* This is a refinement of the paper DAC-21019 presented at the ASME 2001 DETC, Pittsburgh, PA, USA.

1 Introduction

Planar compliant mechanisms transmit force and motion through intentional in-plane elastic deformation. These mechanisms find widespread application in MEMS due to the ease of manufacture, scalability, and robustness offered by their unitized construction. Electrothermal compliant (ETC) actuation of compliant mechanisms uses the thermal strain generated by nonuniform Joule heating to deform the elastic and electrically conductive continuum (Guckel *et al.* 1992). ETC actuation is compatible with both: the manufacturing processes and the voltage/-current operation regime of conventional microelectronics (Comtois and Bright 1996). Hence ETC mechanisms are ideal for applications involving integration of micromechanical and microelectronic systems on the same chip.

The electrothermal actuators developed by Guckel *et al.* (1992) and Que *et al.* (1999), among others, were based on intuitive designs. Moulton and Ananthasuresh (2001) introduced a level of functional abstraction by proposing a building block approach to the synthesis of ETC microactuators. In this approach, building blocks for simple motions are combined to yield more complex ETC micromechanisms. The feasibility of using ETC devices in microsystems demonstrated by such intuitive designs drives the need for a systematic method to design these devices. It is expected that systematic design methods will make the design of ETC devices transparent to the user and thus spur their use in MEMS.

The ETC design problem entails the determination of the geometric form of the device that meets certain design specifications. The specifications include where the device is mechanically anchored, between what portions of the boundary a voltage is applied, and at what point and in what direction deformation is desired. Ananthasuresh (1994), Frecker *et al.* (1997), and Sigmund (1997), among others, have used continuum-element-based topology optimization for the systematic synthesis of optimal topologies for mechanically actuated compliant mechanisms. Saxena and Ananthasuresh (2000) and others have

used the frame-element-based topology optimization approach for designing mechanically actuated compliant mechanisms. The continuum-element-based approach has already been applied to the synthesis of ETC mechanisms (Jonsmann *et al.* 1999; Yin and Ananthasuresh 2001). This paper extends the frame-element-based approach for the topology synthesis of ETC devices.

Any topology optimization process involves discretization of the design domain into elements. The optimization process selectively removes elements from the domain to define an optimal topology for the design objective. In the frame-element-based approach, the design domain is discretized into a network of frame elements called the ground structure. For synthesis of ETC mechanisms, the frame elements in the ground structure are replaced by *line elements*. A *line element* is a one-dimensional model of the electrical, thermal, and elastic behavior of a beam-like continuum. The continuum element method uses a fictitious material density as the design variable. In contrast, the line element approach uses the in-plane width of the line elements as the design variable. The out-of-plane thickness is fixed so that it is compatible with microfabrication processes, which make it difficult to vary device thickness continuously.

The motivation for using the line-element-based ground structure approach stems from the advantages it brings to the ETC synthesis problem. First, it allows for a coarser subdivision of the design domain than the continuum element approach for the same resolution of shape definition. Hence the line-element-based formulation reduces the computational burden for the synthesis procedure without compromising sharpness of the shape definition. Second, the resulting geometry adheres to the original discretization and so is clean and easy to fabricate using photolithography-based microfabrication processes. Third, it is not necessary to interpolate thermophysical properties between existing and nonexisting states in the line element approach, unlike in the material distribution approach. Fourth, it helps to model surface heat transfer more easily than the material distribution approach. This important point is elaborated next.

Mankame and Ananthasuresh (2001) argued that the accurate modeling of surface heat transfer by convection and radiation is important in ETC devices by giving an example of an ETC device whose behavior was *qualitatively* different when surface heat transfer was modeled than when it was ignored. Since surface phenomena dominate bulk ones in MEMS, it is expected that key response variables like the deformation, consumed power, and maximum temperature in the device will be significantly different when surface heat transfer is modeled from when it is not. Therefore, to make topology-optimized ETC devices practically useful, surface heat transfer should be included in the analysis models used for topology optimization.

It is difficult to model surface heat transfer accurately in the continuum element approach because the number, shape, and sizes of holes are not specified a priori as new faces arise and disappear during the iterative optimization procedure. Compared to the top and bottom faces, side walls pose greater difficulty in handling surface heat transfer in the continuously varying topologies. Mankame and Ananthasuresh (2001) report that heat transfer from side walls cannot be ignored even for thin laminar structures because the surface heat transfer coefficient from the side walls at the micro (area $< 1\,\mathrm{mm}^2$) and the meso ($1 < \mathrm{area} < 10\,\mathrm{mm}^2$) scale is much higher than that from the top or bottom surface. This has important implications for the synthesis procedure because compliant mechanisms obtained from optimization are known to have narrow regions that serve as flexures. Since these narrow flexures often experience high stresses, they are common locations for device failure. At these flexures the overall surface heat loss from the side walls is much higher than from the top or bottom surfaces. Hence it is important to model the surface heat transfer at these critical regions accurately in the optimal design of ETC mechanisms.

Top and bottom surface heat transfer can be readily modeled in both the line and continuum element approaches by multiplying the heat transfer coefficient by the design variable. However, modeling sidewall surface heat transfer within the topology optimization framework is more involved. Yin and Ananthasuresh (2001) devised a novel scheme to model convective heat transfer from sidewall surfaces. The scheme makes the analysis procedure substantially more complex and also compromises the accuracy when some elements are in their *intermediate* (i.e., between the existence and nonexistence) states. The ground-structure-based line element approach avoids these difficulties elegantly. The location, thickness, and length of all the elements are specified a priori. Only the width is varied during optimization. Therefore, the area of the side walls remains constant. The heat transfer from top and bottom surfaces varies linearly with the width of the element and is properly accounted for at every step of the optimization process. Ideally, when the width of the element goes to zero, its thermal resistance becomes very high and hence only an infinitesimal amount of heat enters the element.

The thermophysical properties of the workpiece influence the behavior of the ETC, manipulating it. As an

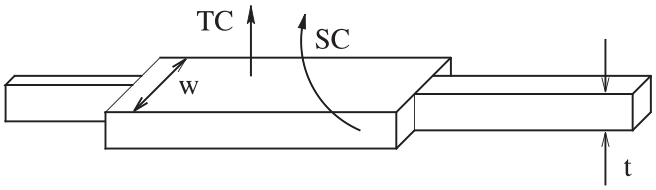

Fig. 1 Schematic of three line elements to show that accurate modeling of convection is easy even in topology optimization because width of the element is the optimization variable. w: in-plane width, t: thickness, TC: top and under surface heat transfer, SC: sidewall heat transfer

example, the electrical and thermal conductivities of the workpiece control the electrical and thermal boundary conditions at the output port of the ETC device. Several interesting effects can be studied by modeling the workpiece also as a line element. These studies are particularly useful for ETC microdevices, which are typically made of a semiconductor-like silicon. In this paper, we study the influence of the interdependency of the output(i.e., workpiece) elastic stiffness, electrical resistance, and thermal resistance on the resulting optimal design of an ETC device, when a rectangular cross section beam in its axial compression mode is used as a model for the workpiece.

Since optimal designs for a number of design specifications can yield roughly similar behavior, the specifications can be revised if significant benefits are forthcoming. As an example, the evolution of optimal topology of an ETC device as the direction of the desired output is varied is studied.

The remainder of this paper is organized as follows. The static equilibrium equations for the coupled electrothermoelastic boundary value problem governing the operation of an ETC device and the formulation of the optimization problem are discussed in Sect. 2. The design sensitivity calculations are presented in Sect. 3. Section 4 covers the design examples and discussion. The last section summarizes the key features of this work and outlines the directions for future efforts.

2
Formulation of the problem

2.1
Governing equations

A general ETC device can be modeled by a set of coupled boundary value problems spanning the electrical, thermal, and elastic energy domains. The domain to be analyzed is represented by the region Ω in Fig. 2. The subscripts E, T, and M refer to electrical, thermal, and elastic boundary conditions, respectively, while the subscripts "e" and "n" indicate, respectively, Dirichlet and Neumann (or mixed) type boundary conditions. A part of the boundary is denoted by Γ, while a generalized traction is denoted by f.

Let $\mathrm{v}(\mathbf{r})$, $\mathrm{T}(\mathbf{r})$, and $\mathbf{u}(\mathbf{r})$ be, respectively, the voltage, temperature, and displacement at a point in the domain whose position is indicated by $\mathbf{r}$. These are the independent variables in the electrical, thermal, and elastic energy domains, respectively. Since linear finite element analysis is used in the synthesis procedure for evaluating the device behavior, the relevant governing equations will be presented in discretized form. The linearized problem for a planar ETC device fabricated from a material that is homogeneous and isotropic in all three energy domains can then be formulated in the following manner.

The boundary value problem in the electrical energy domain is stated in discretized form as

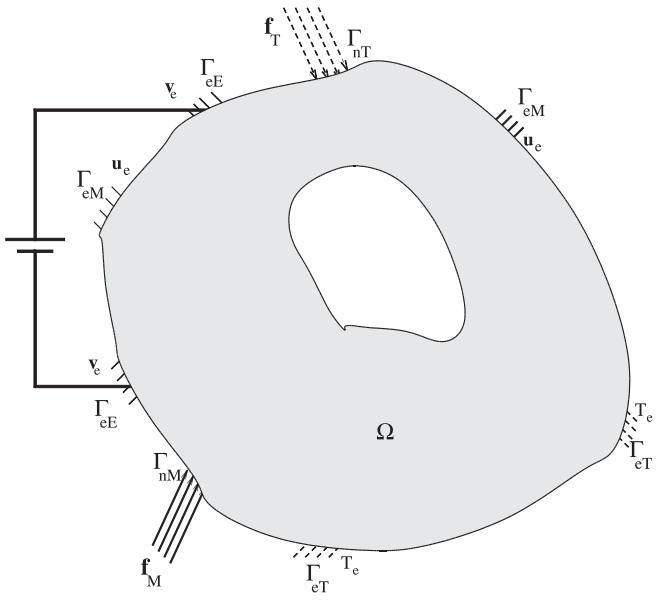

Fig. 2 Schematic of the design domain over which the electro-thermal-elastic boundary value problem is defined.
$\mathrm{v_e}$: the voltage specified on Γ_{eE},
$\mathrm{T_e}$: the temperature specified on Γ_{eT},
$\mathrm{u_e}$: the displacement specified on Γ_{eM},
$\mathrm{f_T}$: the surface heat flux on Γ_{nT},
$\mathrm{f_M}$: the surface traction on Γ_{nM}

$$\mathsf{K}_{\mathrm{e}}\mathbf{v} = \mathbf{0}\,, \quad v = \mathrm{v_e} \text{ on } \Gamma_{\mathrm{eE}}\,, \tag{1}$$

where K_{e} is the electrical conductivity matrix and $\mathbf{v}$ the column vector containing nodal voltages.

The thermal boundary value problem is formulated in discretized form as

$$\mathsf{K}_{\mathrm{T}}\mathbf{T} = \mathbf{Q}\,, \quad \mathrm{T} = \mathrm{T_e} \text{ on } \Gamma_{\mathrm{eT}}\,, \tag{2}$$

where K_{t} is the effective thermal conductivity matrix for the discretized domain comprising heat conductance and surface heat loss effects. The nodal temperature vector is denoted by $\mathbf{T}$. The nodal heat load vector $\mathbf{Q}$ comprises Joule volumetric heat generation and the convective heat loss from the surface. The Joule heat generation is a function of the nodal voltage ($\mathbf{v}$) and the electrical conductivity of the material (k_{e}).

The boundary value formulation for static elastic equilibrium is given as

$$\mathsf{K}_{\mathrm{m}}\mathbf{u} = \mathbf{f}_{\mathrm{M}}\,, \quad u = \mathrm{u_e} \text{ on } \Gamma_{\mathrm{eM}}\,, \tag{3}$$

where K_{m} is the elastic stiffness matrix of the domain and $\mathbf{u}$ is the nodal displacement vector. The mechanical load due to the thermal strains induced by electrical heating is represented by the vector $\mathbf{f}_{\mathrm{M}}$.

This paper does not consider the temperature dependence of thermophysical properties and radiation as a mode of surface heat transfer, although the latter is not difficult to implement in the framework presented here. A linear constitutive elastic law and small displacements are assumed. The model used for this work is thus

a linearized approximation to the full nonlinear boundary value problem. The rate of thermoelastic deformation is small for a DC excitation of the domain. Therefore, the contribution of heat generated by dissipation of the work of deformation to the internal heat generation is negligible as compared with the heat generated by resistive heating. This, together with the assumed temperature independence of thermophysical properties, decouples the boundary value problems in the three energy domains (Kovalenko 1970). The electric, thermal, and elastic boundary value problems can then be solved separately in that order.

2.2 Finite element analysis

The objective function for the optimization problem posed in the next subsection is computed by a linear FE analysis using line elements. A one-dimensional element for the electrical and thermal analysis and a Euler–Bernoulli frame element for the elastic analysis constitutes a *line element*. An example of a design domain and its discretization using line elements is shown in Fig. 3. The discretized domain or ground structure is a mosaic of unit cells each of which comprises eight line elements connecting four nodes at the corners and the single node at the center of the unit cell (Saxena and Ananthasuresh 2000). Line elements used in this paper have a rectangular cross section characterized by the in-plane width w, out-of-plane thickness t, and length l. The electrical and thermal analyses are one-dimensional if the values for w, t, and l are chosen such that gradients of the potential (voltage and temperature) exist only along the axial direction. This condition is satisfied if the values of w and t are small as compared with l. For static in-plane bending, the Bernoulli beam is a one-dimensional approximation of a three-dimensional continuum that can resist axial and shear forces as well as bending moments. The Bernoulli beam approximation neglects shear strain energy in comparison with the bending strain energy. The error introduced by this approximation is proportional to $(w/l)^2$ (Shames and Dym 1985). Hence if we choose element proportions such that the maximum value of w/l is less than 0.2, the one-dimensional approximation is reasonable for all three energy domains.

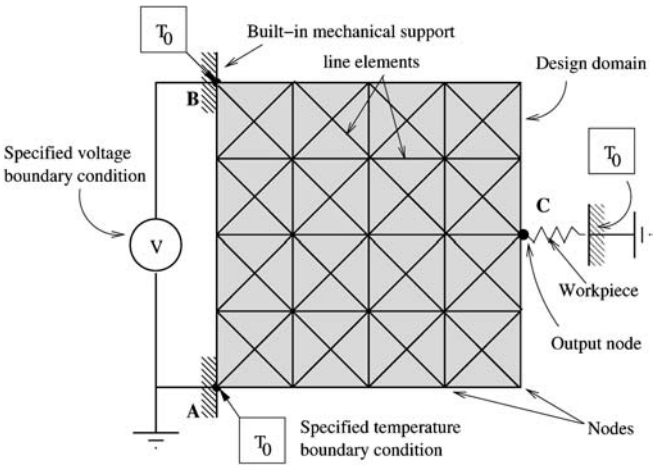

Fig. 3 The design domain, boundary conditions and workpiece location and orientation for design Example 1. The overlaid dark lines indicate the ground structure that discretizes the design domain

2.3 Formulation of the optimization problem

The ratio type multicriteria objective function proposed by Frecker *et al.* (1997) is used to simultaneously maximize the flexibility and stiffness of the ETC mechanism. This objective function is defined in Eq. 4, where *MSE* is the mutual strain energy corresponding to the thermal and unit elastic dummy loads and *SE* is the strain energy due to the thermal loading alone. The chosen objective function f, therefore, captures both attributes: motion transmission and force transmission (Ananthasuresh 1994) required of an ETC mechanism.

The design variable (i.e., in-plane width of an element w) is bounded by the side constraints $w_{\min}$ and $w_{\max}$. The upper bound is chosen such that $w_{\max}/l_{\min}$ is less than 0.2. The lower bound $w_{\min}$ is chosen to be some small number dictated by numerical considerations. The nodal coordinates, applied voltage, material properties, out-of-

Table 1 Parameters used in the synthesis procedure

Symbol	Units	Description	Value
ρ	Ω-m	Electrical resistivity	2.3×10^{-5}
k_{th}	W m^{-1} K^{-1}	Thermal conductivity	141.2
α	K^{-1}	Coefficient of linear thermal expansion	2×10^{-6}
T_∞	K	Ambient temperature	300
h	W m^{-2}	Film coefficient (*approximate*)	250
T_0	K	Workpiece ground temperature	300
E	N m^{-2}	Young's modulus	169×10^9
$w_{\min}$	m	Lower bound on width	1×10^{-6}
$w_{\max}$	m	Upper bound on width	25×10^{-6}
$\mathbf{w}_0$	%	Uniform initial guess	15
V^*	%	Volume constraint	20
R_{e}	Ω	Workpiece electrical resistance	3.1×10^4
R_{t}	K W^{-1}	Workpiece thermal resistance	9.5×10^6
K_{m}	N m^{-1}	Workpiece stiffness	3×10^4
v_0	V	Workpiece ground potential	0

plane thickness t, output spring properties, and imposed boundary conditions are considered as part of the problem specification.

The optimization problem can then be posed as

$$\underset{\mathbf{w}}{\text{Min}} \quad f = \frac{-MSE}{SE} \tag{4}$$

subject to

governing equations in $(1, 2, 3)$,

$w_{\min} \le w_{\mathrm{i}} \le w_{\max} \quad \forall \mathrm{i} \qquad \text{(side constraint)}$,

$$\left(\sum_{\mathrm{i}} w_{\mathrm{i}} l_{\mathrm{i}}\right) t \le V^* \qquad \text{(resource constraint)},$$

where $\mathbf{w}$ is the vector $[w_{\mathrm{i}}]$ of design widths, l_{i} is the length of element i, t is the out-of-plane thickness, and V^* is the maximum permissible volume for the design. The side and volume constraints are both linear in the design variables. This simplifies the optimization process considerably. The constrained nonlinear minimization algorithm `fmincon` from the the Matlab optimization tool box (Coleman *et al.* 1999) was used for the designs presented in this paper. Table 1 contains values assigned to various parameters for the examples in Sect. 4. Sensitivity analysis, which is a key step in gradient-based continuous optimization methods, is described next.

3 Sensitivity analysis

The elements forming the ground structure are partitioned into the sets $\mathcal{A}$ comprising all elements (i.e., including nondesign elements) and $\mathcal{D}$ comprising only the design elements (i.e., whose width can be varied). The vector of design variables is given as $\mathbf{w} = [w_{\mathrm{i}}],\ w_{\mathrm{i}} \in \mathcal{D}$. Differentiating the objective f in Eq. 4 yields the objective sensitivity as

$$\frac{\partial f}{\partial w_{\mathrm{p}}} = \left(-\frac{1}{SE}\frac{\partial MSE}{\partial w_{\mathrm{p}}} + \frac{MSE}{SE^2}\frac{\partial SE}{\partial w_{\mathrm{p}}}\right). \tag{5}$$

The static equilibrium for the structure under the thermal loads is given by Eq. 3 and under the unit dummy load by Eq. 6. The vector of thermal loads is denoted by $\mathbf{f}_{\mathrm{t}}$, and the nodal dummy load vector is denoted by $\mathbf{f}_{\mathrm{d}}$. The nodal displacement vectors $\mathbf{u}$ and $\mathbf{u}_{\mathrm{d}}$ correspond to $\mathbf{f}_{\mathrm{t}}$ and $\mathbf{f}_{\mathrm{d}}$, respectively:

$$\mathsf{K}_{\mathrm{m}}\mathbf{u}_{\mathrm{d}} = \mathbf{f}_{\mathrm{d}}, \quad u = \mathrm{u_e} \text{ on } \Gamma_{\mathrm{eM}}. \tag{6}$$

The expressions for SE and MSE are given by

$$MSE = \mathbf{u}_{\mathrm{d}}^T \mathsf{K}_{\mathrm{m}} \mathbf{u}, \tag{7}$$

$$SE = \frac{1}{2}\mathbf{u}^T \mathsf{K}_{\mathrm{m}} \mathbf{u}. \tag{8}$$

Differentiation of Eqs. 7 and 8 in conjunction with Eq. 3 yields

$$\frac{\partial MSE}{\partial w_{\mathrm{p}}} = \left(\frac{\partial \mathbf{u}_{\mathrm{d}}}{\partial w_{\mathrm{p}}}\right)^T \mathbf{f}_{\mathrm{t}} + \left(\frac{\partial \mathbf{f}_{\mathrm{t}}}{\partial w_{\mathrm{p}}}\right)^T \mathbf{u}_{\mathrm{d}}, \tag{9}$$

$$\frac{\partial SE}{\partial w_{\mathrm{p}}} = \frac{1}{2}\left[\left(\frac{\partial \mathbf{u}}{\partial w_{\mathrm{p}}}\right)^T \mathbf{f}_{\mathrm{t}} + \left(\frac{\partial \mathbf{f}_{\mathrm{t}}}{\partial w_{\mathrm{p}}}\right)^T \mathbf{u}\right]. \tag{10}$$

The derivatives $\partial \mathbf{u}/\partial \mathbf{w}$ and $\partial \mathbf{u}_{\mathrm{d}}/\partial \mathbf{w}$ can be computed by differentiation of Eqs. 3 and 6 using the standard procedures (e.g., Saxena and Ananthasuresh 2000). The presence of $\partial \mathbf{f}_{\mathrm{t}}/\partial w_{\mathrm{p}}$ in Eqs. 9 and 10 couples the elastic and the thermal sensitivity analyses.

The thermal load vector $\mathbf{f}_{\mathrm{t}}$ is obtained from the elemental thermal strains as

$$\mathbf{f}_{\mathrm{t}} = \sum_{\mathrm{e}\in\mathcal{A}} E_{\mathrm{e}} w_{\mathrm{e}} t \epsilon_{\mathrm{e}} \Gamma_{\mathrm{e}}, \tag{11}$$

and its derivative is given by

$$\frac{\partial \mathbf{f}_{\mathrm{t}}}{\partial w_{\mathrm{p}}} = \sum_{\mathrm{e}\in\mathcal{A}} E_{\mathrm{e}} \Gamma_{\mathrm{e}} \left(t\epsilon_{\mathrm{e}}\delta_{\mathrm{ep}} + w_{\mathrm{e}} t \frac{\partial \epsilon_{\mathrm{e}}}{\partial w_{\mathrm{p}}}\right),$$

$$\delta_{\mathrm{ep}} = \begin{cases} 1 & \text{if } \mathrm{e} = \mathrm{p} \\ 0 & \text{otherwise} \end{cases}, \tag{12}$$

where Γ_{e} is a matrix for transforming between the local and global coordinate systems, E_{e} is the Young's modulus, and ϵ_{e} is the thermal strain for the e-th element. The thermal strain vector and its derivative are given by

$$\boldsymbol{\epsilon} = \sum_{\mathrm{e}\in\mathcal{A}} \epsilon_{\mathrm{e}} = \sum_{\mathrm{e}\in\mathcal{A}} \frac{\alpha_{\mathrm{e}}}{2}\left(\mathrm{T}_1^{\mathrm{e}} + \mathrm{T}_2^{\mathrm{e}}\right),$$

$$\frac{\partial \boldsymbol{\epsilon}}{\partial w_{\mathrm{p}}} = \sum_{\mathrm{e}\in\mathcal{A}} \frac{\alpha_{\mathrm{e}}}{2}\left(\frac{\partial \mathrm{T}_1^{\mathrm{e}}}{\partial w_{\mathrm{p}}} + \frac{\partial \mathrm{T}_2^{\mathrm{e}}}{\partial w_{\mathrm{p}}}\right). \tag{13}$$

The temperatures at the two nodes of the e-th element are denoted by $\mathrm{T}_1^{\mathrm{e}}$ and $\mathrm{T}_2^{\mathrm{e}}$, while α_{e} is the coefficient of linear thermal expansion for the element. The temperature derivatives in Eq. 13 are obtained by differentiating the thermal equilibrium equation Eq. 2 as

$$\mathsf{K}_{\mathrm{t}} \frac{\partial \mathbf{T}}{\partial w_{\mathrm{p}}} = \frac{\partial \mathbf{Q}}{\partial w_{\mathrm{p}}} - \frac{\partial \mathsf{K}_{\mathrm{t}}}{\partial w_{\mathrm{p}}}\mathbf{T}. \tag{14}$$

The heat flux load vector $\mathbf{Q}$ and its derivative are obtained from

$$\mathbf{Q} = \sum_{\mathrm{e}\in\mathcal{A}} \mathbf{Q}_{\mathrm{e}} = \sum_{\mathrm{e}\in\mathcal{A}} \frac{l_{\mathrm{e}}}{2}\left[\frac{\left(v_2^{\mathrm{e}} - v_1^{\mathrm{e}}\right)^2}{R_{\mathrm{e}} l_{\mathrm{e}}} + 2h_{\mathrm{e}}(w_{\mathrm{e}} + t)\mathrm{T}_\infty\right],$$

$$\frac{\partial \mathbf{Q}}{\partial w_\mathrm{p}} = \sum_{\mathrm{e}\in\mathcal{A}} \left\{ \frac{1}{R_\mathrm{e}} \left(v_2^\mathrm{e} - v_1^\mathrm{e}\right) \left(\frac{\partial v_2^\mathrm{e}}{\partial w_\mathrm{p}} - \frac{\partial v_1^\mathrm{e}}{\partial w_\mathrm{p}} \right) + \left[\frac{l_\mathrm{e} \left(v_2^\mathrm{e} - v_1^\mathrm{e}\right)^2}{2 R_\mathrm{e} w_\mathrm{e}} + l_\mathrm{e} h_\mathrm{e} \mathrm{T}_\infty \right] \delta_\mathrm{ep} \right\},$$

$$R_\mathrm{e} = \frac{l_\mathrm{e} \rho_\mathrm{e}}{w_\mathrm{e} t}\,, \tag{15}$$

where $\mathbf{Q}_\mathrm{e}$ is the elemental heat flux load, v_2^e and v_1^e are the nodal potentials at the two nodes of the element, R_e is the electrical resistance, T_∞ is the ambient temperature, l_e is the length, h_e is the film heat transfer coefficient, and ρ_e is the electrical resistivity for the e-th element. The nodal potential derivatives in Eq. 15 are obtained by differentiation of the static electric potential equilibrium equation Eq. 1 as

$$\mathsf{K}_\mathrm{e} \frac{\partial \mathbf{v}}{\partial w_\mathrm{p}} = -\frac{\partial \mathsf{K}_\mathrm{e}}{\partial w_\mathrm{p}} \mathbf{v}\,. \tag{16}$$

The derivatives of K_e, K_t, and K_m can be computed from the respective equations. The objective sensitivity can be computed by gathering results from Eqs. 9–16 into Eq. 5.

4 Design examples and discussion

This section covers five design examples whose objectives are briefly described below.

1. Compare results obtained by the line element approach with both intuitive designs and designs from the continuum element approach reported in the literature.
2. Study the influence of the electrical, thermal, and elastic nature of ground supports on the resulting optimal designs.
3. Study the variation in the resulting optimal topologies when the orientation of output displacement and force are varied.
4. Illustrate the influence of the interdependence of electrical and thermal resistances and elastic stiffness for a given workpiece geometry on the resulting optimal designs.
5. Demonstrate the ability of the synthesis procedure to generate nonintuitive designs.

Table 1 summarizes the material properties, mesh details, and other constants common to all examples unless specified otherwise. All material properties are those for p-doped single-crystal silicon at 300 K. The design domain is 1.4 mm square with thickness $t = 2\,\mu$m. The anchors (i.e., the locations where the domain is mechanically attached to ground) are always considered to be at ambient temperature. The output spring is assumed to have a high thermal and electrical resistance as noted in Table 1, except in the case of example 4.

The average of the values at the two nodes of an element is plotted as the constant value for an element in the grayscale plots for the temperature and electrical voltage distributions. The darkness of the shade is proportional to the normalized value of the variable. In the displacement field plot, the elements whose widths have reached w_min are shown dotted, while the remaining elements are displayed with relatively normalized widths. Elements in gray have their widths within the design limits, and the black elements have reached the upper design limit. The dashed thick black line is the workpiece modeled as an output spring directed along the line of action of the specified output displacement. The undeflected configuration is shown in gray, while the deflected configuration is overlaid in black. A displacement magnification factor of 50 is used for generating the displacement field plots. The range of element widths and temperature are both discretized into eight ranges for plotting. Thus the reader must bear in mind while interpreting the plots that small discrepancies due to numerical precision may cause two approximately equal values to fall into different but adjacent intervals.

4.1 Example 1

Figure 3 shows the schematic of the problem specification. A voltage of 10 V is applied across nodes A and B, which are also locations where the domain is mechanically fixed to the ground. The topology resulting from the optimal synthesis is shown in Fig. 4. The value of the objective function for the optimal design as f and for the starting guess as f_0 is listed in the caption.

The topology obtained is remarkably similar to "bent-beam" actuators (Fig. 4) reported in the literature. The temperature distribution (Fig. 5) shows localized heating in the two "legs", while the output port remains nearly at ground temperature. The temperature and displacement fields together suggest a kinematically equivalent configuration as shown in Fig. 6.

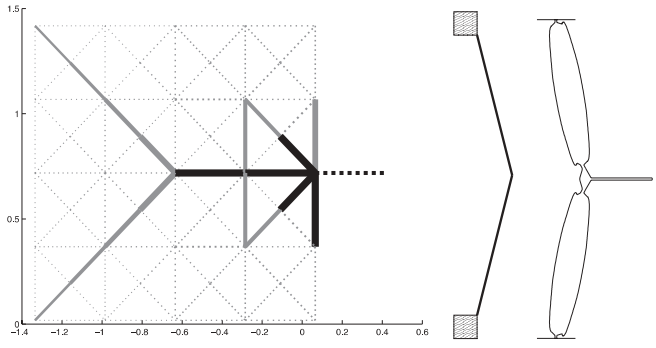

Fig. 4 Optimal topology for Example 1 (left): $f = -6.977$, $f_0 = 0.45$. Intuitive design (Que *et al.* 1999) (center) and continuum element design (Jonsmann *et al.* 1999) (right) for ETC devices with similar functional requirements

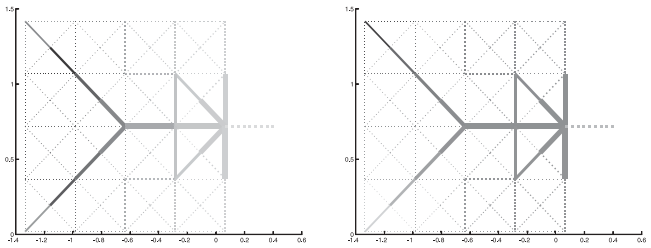

Fig. 5 Temperature distribution (left) and electric potential distribution (right) for Example 1

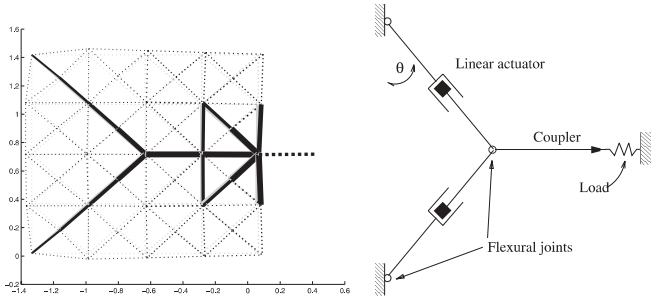

Fig. 6 Original and deflected configurations for Example 1 (left) and a kinematically equivalent mechanism (right) for this device

The chosen ground structure restricts element orientations to 0°, 45°, and 90°. This is unlike the continuum approach where any orientation of design geometry is obtainable, though there is a significant concomitant increase in the problem size. The restriction results in an inclination $\theta = 45°$ (Fig. 6) for the "legs" of the optimal topology in Fig. 4. The value of θ in the other designs shown in the figure is smaller ($< 20°$). This drawback can be readily remedied by either modifying the unit cell to incorporate additional elements having different inclinations or by using the topology generated by this scheme as input to a geometrical optimization procedure that optimizes the nodal coordinates for elements in the design (Hetrick and Kota 1999).

4.2 Example 2

A voltage of 10 V is applied across nodes A and B in Fig. 7. Node C is connected to ground by a support whose elastic and electrothermal properties are varied to study their influence on the resulting optimal topology.

When the support node C is a hinge connection that is electrically and thermally insulated from the ground, the result of the synthesis for $\theta = 135°$ is shown in Fig. 7.

In the next example, node C in the schematic shown in the top panel of Fig. 7 is electrically and thermally

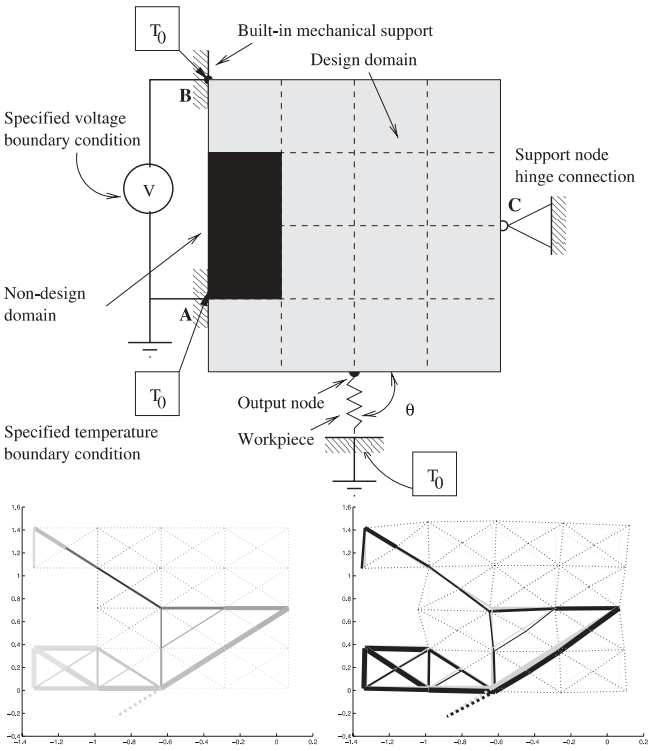

Fig. 7 Schematic of design specification for Example 2. Only the unit cells are indicated by overlaid dashed lines (top). $f = -17.7$, $f_0 = 6.67$. Temperature distribution (bottom left) and displacement field (bottom right)

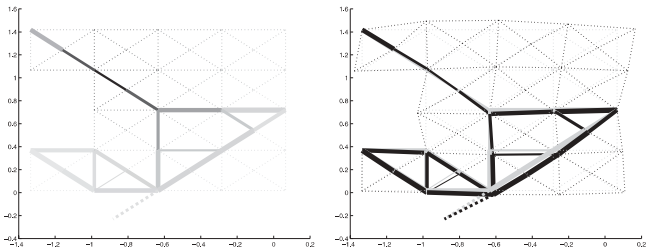

Fig. 8 Temperature distribution for Example 2b (left) and its associated displacement field; $f = -11.17$, $f_0 = 1.33$ (right)

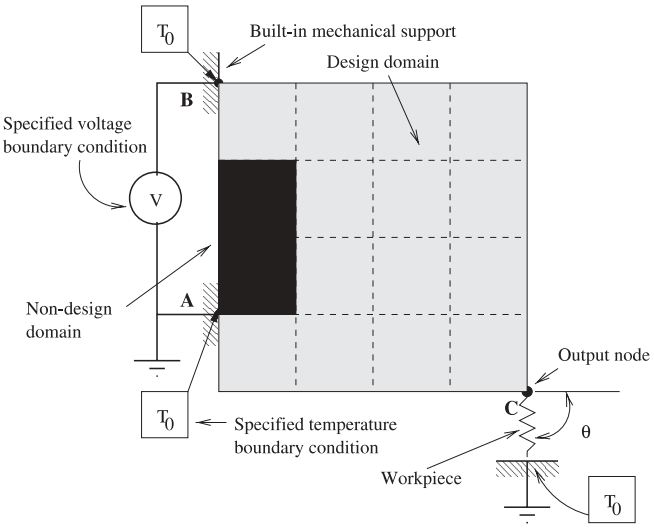

Fig. 9 The design domain, boundary conditions and workpiece location and orientation for design Example 3

grounded, but it now has a "built-in" or fixed mechanical boundary condition. The inclination of the workpiece is retained at $\theta = 135°$.

4.3 Example 3

This set of designs illustrates the change in optimal topologies resulting from a change in the orientation of the output spring. A voltage of 10 V is applied across nodes A and B, while the workpiece is connected at node C, as shown in Fig. 9.

The inclination θ of the workpiece with the horizontal is varied from 45° to 135°. The resulting output topologies are shown in Fig. 10 for some salient designs.

4.4 Example 4

This set of designs illustrates the influence of the interdependence of electrical resistance, thermal resistance, and the elastic stiffness of the workpiece on the resulting optimal topologies.

The electrical resistance (R_e), thermal resistance (R_t), and elastic stiffness (K_m) of the workpiece depend on its material properties and shape. In general, these properties are coupled by the geometry and cannot be chosen independently for a homogeneous workpiece. As an example, if the workpiece is physically modeled as a homogeneous prismatic beam in axial compression, R_e and R_t are proportional to (l/A), where l is the length and A is the area of cross section of the beam. However, K_m is proportional to (A/l). Thus increasing the output elastic stiffness by a factor of n results in reducing the output electrical and thermal resistance by the same factor.

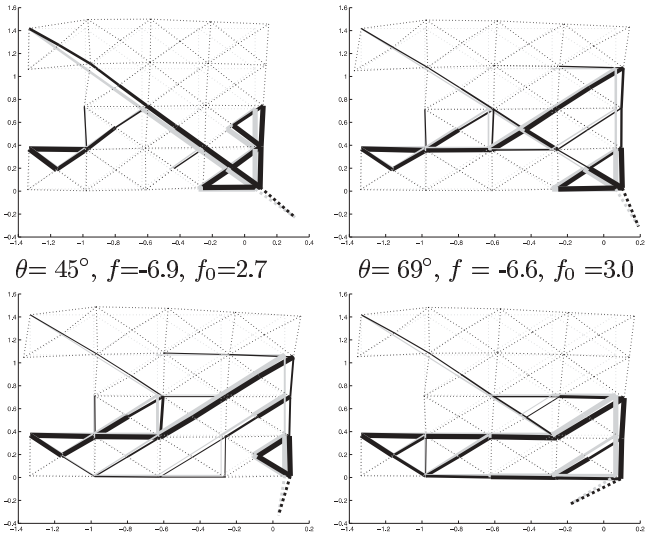

θ= 45°, f=-6.9, f_0=2.7 θ= 69°, f = -6.6, f_0 =3.0

θ= 95.7°, f=-4.3, f_0=3.9 θ= -135°, f = -5.6, f_0 =4.2

Fig. 10 Original and deflected configurations for the designs in Example 3

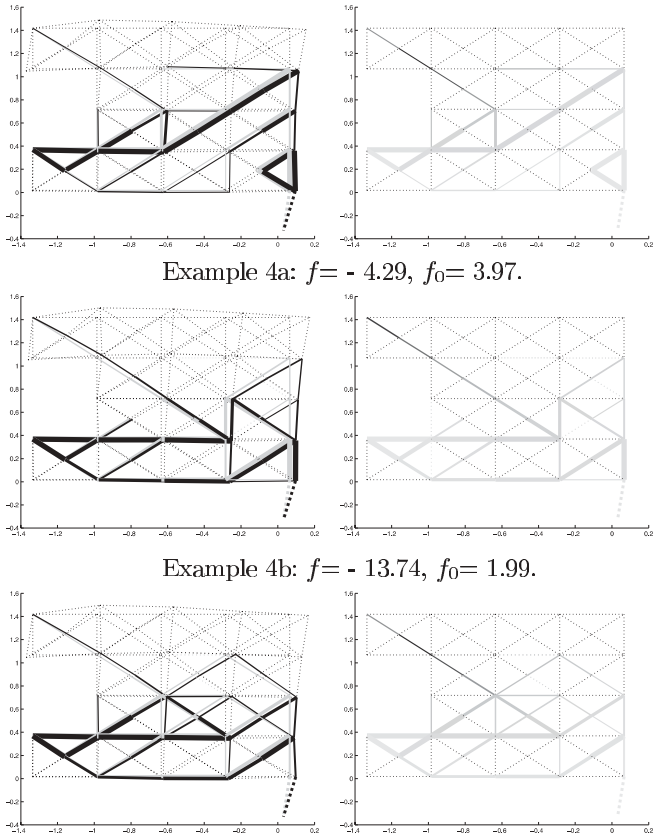

Example 4a: f= - 4.29, f_0= 3.97.

Example 4b: f= - 13.74, f_0= 1.99.

Example 4c: f= - 1.22, f_0= 0.51.

Fig. 11 Deflected configurations for Example 4; (left column) and the associated temperature fields (right column)

The schematic for the problem specification are the same as in Fig. 9 with $\theta = 95°$. A voltage of 10 V is applied across nodes A and B. The workpiece is modeled as a prismatic beam of rectangular cross section in axial compression. The values of K_m, R_e, and R_t in the figure captions are expressed in N/m, Ω, and K/W, respectively.

The first example in this set uses the reference values given in Table 1; $K_m = 3.0 \times 10^4$, $R_e = 3.1 \times 10^4$, and $R_t = 9.5 \times 10^6$. It is assumed that the workpiece is constructed from multiple materials to enable the values of K_m, R_e, and R_t to be chosen independently. The resulting temperature and displacement fields are shown in the top panel of Fig. 11.

If the workpiece is made of uniformly p-doped single-crystal silicon, using the material properties listed in Table 1 leads to $K_m = 1.2 \times 10^4$, $R_e = 3.1 \times 10^2$, and $R_t = 9.5 \times 10^4$ for a workpiece of the same size as in example 4a. The results for this set of workpiece properties are plotted in the center panel of Fig. 11

If the dimensions of the prismatic beam modeling the workpiece are altered to reduce the electrical and thermal resistance by one order of magnitude, the elastic output stiffness will increase by one order of magnitude, as explained above. The corresponding values for the work-

piece made of uniformly doped single crystal silicon are $K_{\mathrm{m}} = 1.2 \times 10^5$, $R_{\mathrm{e}} = 3.1 \times 10^1$, and $R_{\mathrm{t}} = 9.5 \times 10^3$. The results for this case are given in Fig. 11.

4.5 Example 5

The designs in this example illustrate the ability of the synthesis procedure to generate nonintuitive solutions. A voltage of 10 V is applied across nodes A and B in Fig. 12, while the workpiece is connected at node E. The desired direction of output is to the left, as indicated by the orientation of the workpiece. Nodes C and D are connected to ground by supports, whose elastic and electrothermal properties are varied for the different designs.

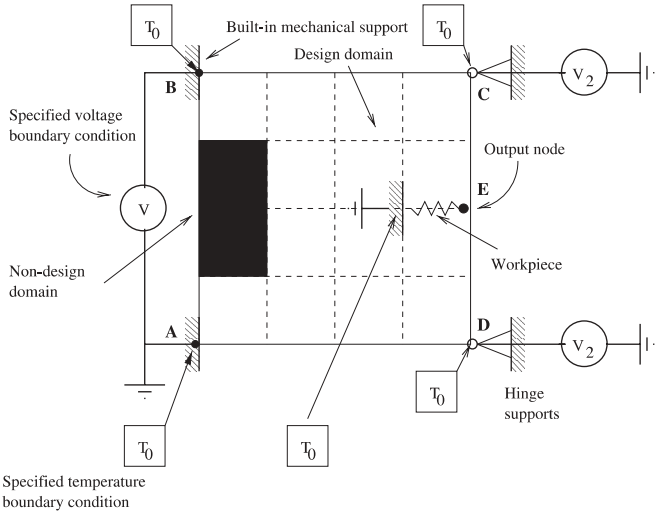

Fig. 12 Schematic of the design specification for Example 5

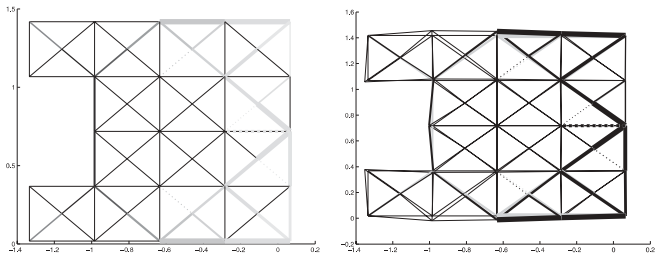

Example 5a: f=-7.26, f_0=9.59.

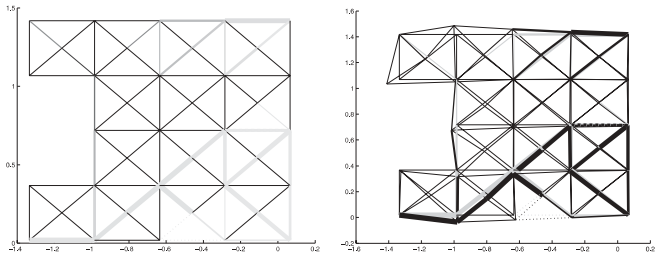

Example 5b: f=-4.48, f_0=5.52.

Fig. 13 Temperature fields (left column) and associated displacement fields (right column) for the designs in Example 5

In Fig. 12, nodes C and D are thermally grounded hinge connections that are maintained at $\mathrm{v}_2 = 5\,\mathrm{V}$ to make the problem specification symmetric. The optimal topology for this problem specification and the corresponding temperature and displacement fields are also shown in the top panel of Fig. 13.

Now consider nodes C and D from Fig. 12 to be thermally and electrically grounded and mechanically fixed. The problem specification is now asymmetric because of the asymmetry in the electric potential field. The resulting optimal topology and the corresponding temperature and displacement fields are also asymmetric, as shown in the bottom panel of Fig. 13.

4.6 Discussion

In all the above examples, the heating was localized to a small region of the mechanism. The localized heating reduces the response time of the actuator, but unfortunately it also renders those regions susceptible to elastic failure due to softening of the material at higher temperatures.

The output port was close to ambient temperature, even when the output electrical and thermal resistances were high. This is very important from the applications point of view.

The examples used thermophysical properties for single-crystal silicon, which is anisotropic in nature. The elastic constants for {100}-cut single-crystal silicon in two dimensions are $\mathcal{C}_{11} = 166\,\mathrm{GPa}$ and $\mathcal{C}_{12} = 64\,\mathrm{GPa}$. Using the expressions in Senturia (2001), the axial Young's modulus (E) can be computed for an element oriented along any general direction in the plane. The appropriate value of E can then be used for any element in the superstructure. Then the framework derived for an isotropic material can still be used with proper bookkeeping. However, in the foregoing examples a constant E was used for simplicity.

The appearance of poorly connected (*dangling*) elements in the topology was studied by computing finite sensitivities and tracking the evolution of the design in example 1. The finite sensitivity for the e-th element was computed as $\Delta_{\mathrm{e}} = (f - f^*)/(w_{\mathrm{e}} - w_{\mathrm{e}}^*)$. The value of the objective function was f when the width (w_{e}) of the element was set to $w_{\min}$. This corresponds to the topology obtained if that element was removed from the optimal design produced by the synthesis. The element width and the objective function for the optimal design are indicated by asterisks(*). It is noted that:

- Δ_{e} was *negative* for the apparent *dangling* elements, indicating that the objective function would increase if the element were removed.
- It was difficult to distinguish the functional and *dangling* elements on the basis of their Δs.

The dangling elements appear at some early point in the optimization process and then are carried unaltered

through the rest of the process. Thus it appears that these elements serve some purpose (e.g., heat dissipation) or are an artifact of the nonconvexity of the design space.

5 Conclusion

A *line-element*-based approach to topology synthesis of electrothermal compliant(ETC) mechanisms was presented. The use of element in-plane width as the design variable obviated the use of a constitutive model for interpolating electrical and thermal properties as a function of a fictitious density. The line element approach also facilitated the implementation of the surface heat transfer from the vertical side walls in a straightforward manner. Linear volume and side constraints yielded reasonable and intuitively explainable results. The method generated designs that are easy to fabricate. The ground structure domain discretization in conjunction with use of line elements facilitated the use of a coarse mesh, which resulted in a low computational cost. The presented approach therefore provides a computationally efficient alternative to the continuum-element-based approach for the synthesis of ETC mechanisms. An example was used to demonstrate the fact that the results from the line-element-based approach compare favorably with results from the continuum-element-based approach. Various examples were used to illustrate the influence of the orientation of the output spring, the effect of the electrical and thermal resistance of the output spring on the resulting topologies, and the ability of the procedure to generate nonintuitive designs.

The appearance of poorly connected elements in the generated designs was studied. Future efforts will focus on techniques to identify such elements and eliminate them. Another open issue concerns strategies to avoid localized heating in thin members carrying a high axial load.

Acknowledgements The work was supported by NSF Grant DMI 97-33916 CAREER. The authors wish to thank Professor P.S. Ayyaswamy, University of Pennsylvania, for discussions on modeling heat transfer from ETC devices.

References

Ananthasuresh, G.K. 1994: A new design paradigm for micro-electromechanical systems and investigations on the compliant mechanisms synthesis. *Ph.D. dissertation, The University of Michigan, Ann Arbor, MI, USA*

Coleman, T.; Branch, M.A.; Grace, A. 1999: *Optimization Toolbox User's Guide*, **Ver. 2**. The Mathworks Inc, Natick, MA 01760-1500, USA

Comtois, J.; Bright, V. 1996: Surface micromachined polysilicon actuator arrays and applications. *Technical Digest of the 1996 Solid State Sensors and Actuators Workshop, Hilton Head, SC*, June 3–6, 1996, pp. 174–177

Frecker, M.I.; Ananthasuresh, G.K.; Nishiwaki, S.; Kikuchi, N.; Kota, S. 1997: Topological synthesis of compliant mechanisms using multi-criteria optimization. *ASME J. Mech. Des.* **119**, 238–245

Guckel, H.; Klein, J.; Christenson, T.; Skrobis, K.; Laudon, M.; Lovell, E.G. 1992: Thermo-magnetic metal flexure actuators. *Technical Digest of the 1992 Solid State Sensor and Actuator Workshop, Hilton Head, SC*, June 13–16, 1992, pp. 73–75

Hetrick, J.A.; Kota, S. 1999: An energy formulation for parametric size and shape optimization of compliant mechanisms. *ASME J. Mech. Des.* **121**(2), 229–234

Jonsmann, J.; Sigmund, O.; Bouwstra, S. 1999: Compliant electrothermal microactuators. *Proc. of the 1999 IEEE MEMS Conference*, Orlando FL, January 1999, pp. 588–593

Kovalenko, A.D. (translated from Russian by Macvean, D.B.) 1995: *Thermoelasticity. Basic theory and applications*, The Netherlands: Wolters-Noordhoff, Groningen

Mankame, N.D.; Ananthasuresh, G.K. 2001: Comprehensive thermal modelling and characterization of an electro-thermal-compliant microactuator. *J. Micromech. Microeng.* **11**(5), 452–462

Moulton, T.; Ananthasuresh, G.K. 2001: Micromechanical devices with embedded electro-thermal-compliant actuation. *Sensors and Actuators A: Physical* **90**(1–2), 38–48

Que, L.; Park, J.-S.; Gianchandani, Y.B. 1999: Bent-beam electrothermal actuators for high force applications. *Proc. of the 1999 IEEE MEMS Conference*, Orlando FL, January 1999, pp. 31–36

Saxena, A.; Ananthasuresh, G.K. 2000: On an optimal property of compliant topologies. *Struct. Multidisc. Optim.* **19**(1), 36–49

Senturia, S.D. 1985: *Microsystem design*. Kluwer Academic Publishers, USA, pp. 663–664

Shames, I.H.; Dym, C.L. 1985: *Energy and finite element methods in structural mechanics*. USA: Hemisphere Publishing Corp./ McGraw Hill Book Co.

Sigmund, O. 1997: On the design of compliant mechanisms using topology optimization. *Mech. Struct. & Mach.* **25**(4), 493–524

Yin, L.; Ananthasuresh, G.K. 2001: Topology optimization of compliant mechanisms with multiple materials using a peak function material interpolation scheme. *Struct. Multidisc. Optim.* **23**(1), 49–62